3D Angle-of-Arrival Positioning Using von Mises–Fisher Distribution

Henri Nurminen, Laura Suomalainen, Simo Ali-Löytty, and Robert Piché
Tampere University of Technology, Tampere, Finland
Emails: {henri.nurminen, simo.ali-loytty, robert.piche}@tut.fi

Abstract—We propose modeling an angle-of-arrival (AOA) positioning measurement as a 3-dimensional von Mises–Fisher (VMF)-distributed unit vector instead of the conventional normally distributed azimuth and elevation measurements. Describing the 2-dimensional AOA measurement with three numbers removes discontinuities and reduces nonlinearity at the poles of the azimuth–elevation coordinate system. Our computer simulations show that the proposed VMF measurement noise model based approximative Bayesian filters outperform the normal distribution based algorithms in accuracy in a scenario where close-to-pole measurements occur frequently.

Index Terms—positioning; angle-of-arrival; von Mises–Fisher distribution; particle filter; extended Kalman filter

I. INTRODUCTION

Many future positioning systems will use angle-of-arrival (AOA) measurements, as the coming 5G networks can be equipped with antenna arrays that enable measuring the AOA of the received electromagnetic signal [1]. Current commercial applications of AOA positioning include e.g. Bluetooth Low Energy based positioning systems [2]. An AOA measurement consists of two components: azimuth and elevation. A conventional approach is to model the measurements as noisy versions of the true azimuth and elevation [3]–[7], and use extended Kalman fiter (EKF) or unscented Kalman filter (UKF) that assume that the measurement noises of azimuth and elevation follow normal distributions. However, this model is problematic in a number of ways:

1) In this model the solid angle of measurement uncertainty is smaller close to the "pole" directions, i.e. the two directions where azimuth is not defined.
2) The measurement model is highly nonlinear close to the poles and discontinuous in the pole, which makes gradient-based approximations for optimisation and extended Kalman filtering unstable. This problem has been reported to result in divergence of the EKF [4].
3) Rotations of the spherical coordinate system in which the azimuth and elevation are expressed change the measurement error model.

To remedy these problems, we propose expressing the 2-dimensional spherical AOA measurement as a 3-dimensional Cartesian unit vector, and modeling the measurement error with the von Mises–Fisher (VMF) distribution [8], [9]. This idea and its advantages are analogous to modeling a rotation with a 4-dimensional Bingham-distributed unit quaternion instead of a 3-dimensional Euler angle set [10, Ch. 3.10], [11]. We also propose a particle filter (PF) algorithm [12] based on the VMF measurement error model, and EKF [13, Ch. 8.3] and UKF [14] algorithms that approximate the VMF update with the assumption that the unit vector measurement is the true direction's unit vector plus a trivariate normal noise. Our simulations show that the proposed positioning algorithms outperform the conventional algorithms in accuracy. VMF filters have also been proposed in [15]–[18], but in these filters both the state and measurements are VMF-distributed unit vectors.

II. MODELLING OF AOA MEASUREMENT

A. Von Mises–Fisher distribution

The support of the VMF's probability density function (PDF) is the unit (hyper-)sphere. A unit vector $x \in \mathbb{R}^n$ follows the distribution $\text{VMF}(\mu, \kappa)$ with mean direction $\mu \in \mathbb{R}^n$, $\|\mu\| = 1$, and concentration parameter $\kappa \in \mathbb{R}_+$ if its PDF is

$$p(x) = C_\kappa e^{\kappa \mu^\mathsf{T} x}. \tag{1}$$

The larger the parameter κ is, the more the probability mass is concentrated around the direction μ. For $\kappa > 0$ the distribution is unimodal and for $\kappa = 0$ it is uniform on the sphere. For a 3-dimensional variable the normalisation constant is

$$C_\kappa = \begin{cases} \frac{\kappa}{4\pi \sinh \kappa}, & \kappa > 0 \\ \frac{1}{4\pi}, & \kappa = 0 \end{cases}. \tag{2}$$

The VMF distribution is suitable for modelling directional data because a direction can be bijectively mapped to a unit vector. The distribution is rotation invariant in the sense that if $x \sim \text{VMF}(\mu, \kappa)$, then for $y = Rx$ holds $y \sim \text{VMF}(R\mu, \kappa)$ for a rotation matrix R. The PDF of $\text{VMF}(\mu, \kappa)$ is the restriction of the PDF of the multivariate normal distribution $\text{N}(\mu, \frac{1}{\kappa} I_n)$ into the origin-centered unit hyper-sphere [19, Ch. 9.3.2].

B. Comparison of normal and VMF models

In this paper an AOA measurement consists of azimuth measurement $y^{\text{AZI}} \in (-\pi, \pi]$ and elevation measurement $y^{\text{ELE}} \in [-\frac{\pi}{2}, \frac{\pi}{2}]$. We define the equator to be $y^{\text{ELE}} = 0$, the

poles $y^{\text{ELE}} = \pm\frac{\pi}{2}$, and the up direction $y^{\text{ELE}} = \frac{\pi}{2}$. The mapping from an AOA measurement to a unit vector is thus

$$\texttt{toUnitvector}(y^{\text{AZI}}, y^{\text{ELE}}) = \begin{bmatrix} \cos y^{\text{AZI}} \cdot \cos y^{\text{ELE}} \\ \sin y^{\text{AZI}} \cdot \cos y^{\text{ELE}} \\ \sin y^{\text{ELE}} \end{bmatrix}. \quad (3)$$

Given user position $\theta \in \mathbb{R}^3$ and anchor position $s \in \mathbb{R}^3$, the conventional normal distribution based measurement model is

$$y^{\text{AZI}} = \text{atan2}(\theta_2 - s_2, \theta_1 - s_1) + e_{\text{AZI}} \quad (4a)$$
$$y^{\text{ELE}} = \text{atan2}((\theta_3 - s_3), \|\theta_{1:2} - s_{1:2}\|) + e_{\text{ELE}}, \quad (4b)$$

where $e_{\text{AZI}} \sim \text{N}(0, \sigma_{\text{AZI}}^2)$ and $e_{\text{ELE}} \sim \text{N}(0, \sigma_{\text{ELE}}^2)$ are noise terms that are statistically mutually independent and independent from θ, and σ_{AZI} and σ_{ELE} are model parameters. The proposed VMF based measurement model is

$$\texttt{toUnitvector}(y^{\text{AZI}}, y^{\text{ELE}}) \sim \text{VMF}\left(\frac{\theta - s}{\|\theta - s\|}, \kappa\right), \quad (5)$$

where the concentration κ is a model parameter.

C. Conversions between normal and VMF models

In order to compare the normal and VMF based estimation algorithms, we seek a simple rule-of-thumb formula that converts one model to the other. When $\alpha_{x,\mu}$ is the angle between unit vectors x and μ, the PDF of $x \sim \text{VMF}(\mu, \kappa)$ is

$$p(x) \propto e^{\kappa \cos(\alpha_{x,\mu})} \approx e^{\kappa(1 - \frac{1}{2}\alpha_{x,\mu}^2)} \propto \text{N}(\alpha_{x,\mu}; 0, \tfrac{1}{\kappa}), \quad (6)$$

which follows from the second order truncated MacLaurin series of $\cos(\alpha_{x,\mu})$ and holds for small $\alpha_{x,\mu}$. We thus recommend to implement the normal distribution based filters for VMF-distributed errors and VMF based filters for normally distributed errors with the conversion rules

$$[\sigma_{\text{AZI}}^2]_{\text{filter}} = [\sigma_{\text{ELE}}^2]_{\text{filter}} \triangleq \frac{1}{\kappa_{\text{true}}}, \quad \kappa_{\text{filter}} \triangleq \frac{1}{\max\{[\sigma_{\text{AZI}}^2]_{\text{true}}, [\sigma_{\text{ELE}}^2]_{\text{true}}\}}. \quad (7)$$

III. BAYESIAN FILTERING

We assume a normal initial prior $x_0 \sim \text{N}(x_{0|0}, P_{0|0})$ and a linear–normal state transition model for the state $x \in \mathbb{R}^{n_x}$

$$x_k = A_{k-1}x_{k-1} + w_{k-1}, \quad w_{k-1} \sim \text{N}(0, Q_{k-1}), \quad (8)$$

where A_{k-1} is state transition matrix, w_{k-1} is process noise, and Q_{k-1} is process noise covariance matrix. In this paper the state includes the 3-dimensional user position, and the three position components in the state are denoted by $[x_k]_{\text{pos}}$.

In the PF algorithm [20, Ch. 3] random samples ("particles") are generated from the initial prior, propagated in time using the state transition model, weighted using the measurement information, and resampled when the weight concentrates too much. PF is flexible in modeling and can be applied to both normal distribution based measurement model (4) and VMF model (5) without any application-specific tweaks. PF for the VMF model is given in Algorithm 1.

EKF and UKF are nonlinear Kalman filter extensions for state-space models where the noises are normally distributed but the model functions can be nonlinear. Application of

---

Algorithm 1 Particle filter for VMF measurement noise

1: **Inputs:** initial prior $x_{0|0}$, $P_{0|0}$; state-transition model $A_{1:K}$, $Q_{1:K}$; concentration parameter κ; $y_{1:K}^{\text{AZI}}$, $y_{1:K}^{\text{ELE}}$; anchor positions & rotations $s_{1:n_s}$, $R_{1:n_s}$
2: **Outputs:** estimates $x_{k|k}$ for $k = 1, \ldots, K$
3: $x_0^{(i)} \sim \text{N}(x_{0|0}, P_{0|0})$, $\quad w_0^{(i)} \leftarrow \frac{1}{N_p}$ for $i = 1, \ldots, N_p$
4: **for** $k = 1 : K$ **do**
5: $\quad u_j \leftarrow \texttt{toUnitvector}([y_k^{\text{AZI}}]_j, [y_k^{\text{ELE}}]_j)$ for $j = 1, \ldots, n_s$
6: $\quad$ **for** $i = 1 : N_p$ **do**
7: $\quad\quad x_k^{(i)} \sim \text{N}(A_{k-1}x_{k-1}^{(i)}, Q_{k-1})$
8: $\quad\quad \widetilde{w}_k^{(i)} \leftarrow \exp\left(\kappa \sum_{j=1}^{n_s} u_j^\mathsf{T} R_j \frac{[x_k^{(i)}]_{\text{pos}} - s_j}{\|[x_k^{(i)}]_{\text{pos}} - s_j\|}\right) \cdot w_{k-1}^{(i)}$
9: $\quad$ **end for**
10: $\quad w_k^{(i)} \leftarrow \frac{\widetilde{w}_k^{(i)}}{\sum_{j=1}^{N_p} \widetilde{w}_k^{(j)}}$ for $i = 1, \ldots, N_p$
11: $\quad x_{k|k} \leftarrow \sum_{i=1}^{N_p} w_k^{(i)} x_k^{(i)}$
12: $\quad$ **if** $1/\sum_{i=1}^{N_p} (w_k^{(i)})^2 < 0.1 N_p$ **then**
13: $\quad\quad [x_k^{(1:N_p)}, w_k^{(1:N_p)}] = \texttt{resample}(x_k^{(1:N_p)}, w_k^{(1:N_p)})$
14: $\quad$ **end if**
15: **end for**

Algorithm 2 EKF for VMF measurement noise

1: **Inputs:** $x_{0|0}, P_{0|0}$; $A_{1:K}$, $Q_{1:K}$; κ; $y_{1:K}^{\text{AZI}}$, $y_{1:K}^{\text{ELE}}$; anchor positions & rotations $s_{1:n_s}, R_{1:n_s}$
2: **Outputs:** estimates $x_{k|k}$ for $k = 0, \ldots, K$
3: **for** $k = 1 : K$ **do**
4: $\quad x_{k|k-1} \leftarrow A_{k-1}x_{k-1|k-1}$
5: $\quad P_{k|k-1} \leftarrow A_{k-1}P_{k-1|k-1}A_{k-1}^\mathsf{T} + Q_{k-1}$
6: $\quad$ **for** $j = 1 : n_s$ **do**
7: $\quad\quad u_{3j-2:3j} \leftarrow \texttt{toUnitvector}([y_k^{\text{AZI}}]_j, [y_k^{\text{ELE}}]_j)$
8: $\quad\quad d_j \leftarrow \frac{x_{k|k-1} - s_j}{\|x_{k|k-1} - s_j\|}$
9: $\quad\quad [c_k]_{3j-2:3j} \leftarrow R_j d_j$
10: $\quad\quad [C_k]_{3j-2:3j,\text{pos}} \leftarrow \frac{1}{\|x_{k|k-1} - s_j\|} R_j \left(I_3 - d_j d_j^\mathsf{T}\right)$
11: $\quad\quad [C_k]_{3j-2:3j,-\text{pos}} \leftarrow \text{O (zero matrix)}$
12: $\quad$ **end for**
13: $\quad K_k \leftarrow P_{k|k-1}C_k^\mathsf{T}(C_k P_{k|k-1}C_k^\mathsf{T} + \kappa^{-1}I_{3n_s})^{-1}$
14: $\quad x_{k|k} \leftarrow x_{k|k-1} + K_k(u^\mathsf{T} - c_k)$
15: $\quad P_{k|k} \leftarrow P_{k|k-1} - K_k S_k K_k^\mathsf{T}$
16: **end for**

EKF and UKF to the normal model (4) is straightforward, except that the angle wrappings have to be taken into account when computing the angular differences. Because EKF and UKF assume normally distributed measurement noise, they are not applicable to the VMF measurement model (5), but we approximate the VMF model with the model

$$\texttt{toUnitvector}([y_k^{\text{AZI}}]_j, [y_k^{\text{ELE}}]_j) \sim \text{N}\left(\frac{[x_k]_{\text{pos}} - s_j}{\|[x_k]_{\text{pos}} - s_j\|}, \frac{1}{\kappa}I_3\right). \quad (9)$$

and apply the standard EKF and UKF to this model. The details of the EKF are given in Algorithm 2 and the details of the UKF in Algorithm 3.

Algorithm 3 UKF for VMF measurement noise

1: **Inputs:** $x_{0|0}, P_{0|0}$; $A_{1:K}, Q_{1:K}$; κ; $y_{1:K}^{\mathrm{AZI}}, y_{1:K}^{\mathrm{ELE}}$ anchor positions & rotations $s_{1:n_s}, R_{1:n_s}$; filter parameter λ

2: **Outputs:** estimates $x_{k|k}$ for $k = 0, \ldots, K$

3: $\omega_0 \leftarrow \frac{\lambda}{n_x + \lambda}$, $\omega_i \leftarrow \frac{1}{2(n_x + \lambda)}$ for $i = 1, \ldots, 2n_x$

4: **for** $k = 1 : K$ **do**

5: $\quad x_{k|k-1} \leftarrow A_{k-1} x_{k-1|k-1}$

6: $\quad P_{k|k-1} \leftarrow A_{k-1} P_{k-1|k-1} A_{k-1}^{\mathsf{T}} + Q_{k-1}$

7: $\quad \chi_0 \leftarrow x_{k-1|k-1}$

8: $\quad$ **for** $i = 1 : n_x$ **do**

9: $\qquad \chi_i \leftarrow x_{k|k-1} + \sqrt{n_x + \lambda} \cdot [P_{k|k-1}^{\frac{1}{2}}]_{:,i}$

10: $\qquad \chi_{2i} \leftarrow x_{k|k-1} - \sqrt{n_x + \lambda} \cdot [P_{k|k-1}^{\frac{1}{2}}]_{:,i}$

11: $\quad$ **end for**

12: $\quad$ **for** $j = 1 : n_s$ **do**

13: $\qquad u_{3j-2:3j} \leftarrow \texttt{toUnitvector}([y_k^{\mathrm{AZI}}]_j, [y_k^{\mathrm{ELE}}]_j)$

14: $\qquad [v_i]_{3j-2:3j} \leftarrow R_j \frac{[\chi_i]_{\mathrm{pos}} - s_j}{\|[\chi_i]_{\mathrm{pos}} - s_j\|}$ for $i = 0, \ldots, 2n_x$

15: $\quad$ **end for**

16: $\quad \mu_k \leftarrow \sum_{i=0}^{2n_s} \omega_i v_i$

17: $\quad S_k \leftarrow \kappa^{-1} I_{3n_s} + \sum_{i=1}^{2n_x} \omega_i (v_i - \mu_k)(v_i - \mu_k)^{\mathsf{T}}$

18: $\quad D_k \leftarrow \sum_{i=0}^{2n_x} \omega_i (\chi_i - x_{k|k-1})(v_i - \mu_k)^{\mathsf{T}}$

19: $\quad K_k \leftarrow D_k S_k^{-1}$

20: $\quad x_{k|k} \leftarrow x_{k|k-1} + K_k(u^{\mathsf{T}} - c_k)$

21: $\quad P_{k|k} \leftarrow P_{k|k-1} - K_k S_k K_k^{\mathsf{T}}$

22: **end for**

IV. SIMULATIONS

A. Measurement models and filters

We compare the proposed filters based on the VMF and unit vector model (5) with the filters based on the normal distribution and azimuth–elevation model (4). The comparisons rely on numerical simulations computed with MATLAB.

We study two different measurement models, from which the measurements are generated:

Model I The measurements are generated from the normal model (4) such that each direction has a unique azimuth–elevation representation; i.e. if the generated elevation measurement $[y_k^{\mathrm{ELE}}]_j$ is larger than $\frac{\pi}{2}$ (or less than or equal to $-\frac{\pi}{2}$), the elevation is flipped to its supplementary angle $\pi - [y_k^{\mathrm{ELE}}]_j$ (or to the angle $-\pi - [y_k^{\mathrm{ELE}}]_j$) and the azimuth measurement $[y_k^{\mathrm{AZI}}]_j$ is flipped to $\pi - \mathrm{mod}(2\pi - [y_k^{\mathrm{AZI}}]_j, 2\pi)$. The flipping emulates a real-world device's way of assigning a unique value to a direction.

Model II The measurements are generated from the VMF model (5).

We compare four different positioning filters:

AE-nominal normal model (4); with Model I σ_{AZI} and σ_{ELE} are the scale parameters of the distribution from which the data were generated, with Model II σ_{AZI} and σ_{ELE} are determined using (7).

AE-fitted normal model (4); σ_{AZI} and σ_{ELE} fitted as the maximum likelihood parameters given by 10^5 simulated measurements generated for 10^5 random directions.
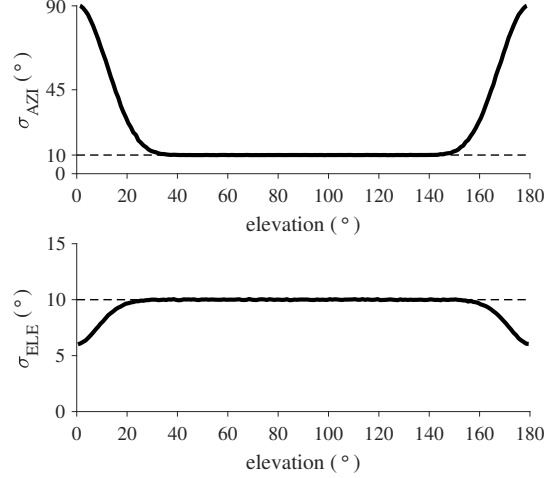

Fig. 1. Standard deviations of the azimuth (upper) and elevation (lower) measurement noises as a function of the elevation in the normal model with the flipping and $\sigma_{\mathrm{AZI}} = \sigma_{\mathrm{ELE}} = 10°$.

AE-adaptive normal model (4); σ_{AZI} and σ_{ELE} chosen as the standard deviations of the normal distribution with flipping at the given elevation; these standard deviations are pre-computed using a grid with 1-degree grid size for the elevation, and shown in Fig. 1.

VMF VMF model (5); with Model I κ is determined using (7), with Model II κ is the concentration parameter of the VMF from which the data were generated.

Note that when a VMF based measurement error model (Model II) is transformed into a normal distribution based model, the exact moment matching solution becomes a non-additive error model, i.e. the distribution of the azimuth and elevation errors is dependent on the true direction. In this view, the AE-fitted model is an approximate moment matching approximation as an expectation value over a random true direction, and the AE-adaptive model is an approximate moment matching approximation for a given direction.

B. Model comparison

In this test we compute the expectations of the normal and VMF log-likelihoods over the distribution $p(y^{\mathrm{AZI}}, y^{\mathrm{ELE}}, \theta)$. The conditional measurement distribution $p(y^{\mathrm{AZI}}, y^{\mathrm{ELE}}|\theta)$ is either the normal distribution with flipping (Model I) or the azimuth–elevation distribution implied by the VMF distribution (Model II), and 3-dimensional position's distribution is the uniform distribution over the unit sphere $p(x) = \frac{1}{4\pi}$. The quantitative goodness of the normal fit is measured with

$$
\begin{aligned}
\mathcal{L}_{\mathrm{N}} = \int_0^\pi \!\! \int_{-\pi}^\pi \!\! \int_{\mathcal{S}_3(1)} & \big[\log \mathrm{N}_{[-\pi,\pi]}(y^{\mathrm{AZI}} - \mathrm{atan}_2(\theta_2, \theta_1); 0, \sigma_{\mathrm{AZI}}^2) \\
& + \log \mathrm{N}_{[0,\pi]}(y^{\mathrm{ELE}} - \mathrm{atan}_2(\theta_3, \|\theta_{1:2}\|); 0, \sigma_{\mathrm{ELE}}^2) \big] \\
& \times p(y^{\mathrm{AZI}}, y^{\mathrm{ELE}}|\theta) \tfrac{1}{4\pi} \, \mathrm{d}\theta \, \mathrm{d}y^{\mathrm{AZI}} \, \mathrm{d}y^{\mathrm{ELE}},
\end{aligned}
\tag{10}
$$

where $\mathcal{S}_3(1)$ is the 3-dimensional unit sphere, and $\mathrm{N}_{\mathcal{A}}$ is the normal distribution truncated to the set $\mathcal{A}$. The goodness of

TABLE I
MODEL COMPARISON

Filter model	Data from Model I		Data from Model II	
	Parameters	$\propto \exp(\mathcal{L})$	Parameters	$\propto \exp(\mathcal{L})$
AE-nominal	$\sigma_{\text{AZI}}=10$ $\sigma_{\text{ELE}}=10$	0.13	$\sigma_{\text{AZI}}=10$ $\sigma_{\text{ELE}}=10$	0.11
AE-fitted	$\sigma_{\text{AZI}}=18$ $\sigma_{\text{ELE}}=10$	0.21	$\sigma_{\text{AZI}}=21$ $\sigma_{\text{ELE}}=10$	0.24
AE-adaptive		0.33		0.30
VMF-nominal	$\kappa=33$	0.32	$\kappa=33$	0.35

the VMF fit is measured with the number

$$\mathcal{L}_{\text{VMF}}=\int_0^\pi\!\int_{-\pi}^\pi\!\int_{\mathcal{S}_3(1)} \big[\log\text{VMF}(\texttt{toUnitvector}(y^{\text{AZI}},y^{\text{ELE}}); \theta, \kappa)$$
$$+ \log(\sin(y^{\text{ELE}}+\tfrac{\pi}{2}))\big]\, p(y^{\text{AZI}}, y^{\text{ELE}}|\theta)\tfrac{1}{4\pi}\,\mathrm{d}\theta\,\mathrm{d}y^{\text{AZI}}\,\mathrm{d}y^{\text{ELE}}. \tag{11}$$

The term $\log(\sin(y^{\text{ELE}}+\frac{\pi}{2}))$ in (11) comes from the transformation from Cartesian space's unit sphere into spherical coordinates domain with radius one. We computed (10) and (11) using Monte Carlo integration with 10^5 samples.

We compare the different models using the model comparison number $\exp(\mathcal{L})$; the higher the model comparison number, the better the model explains the generated data. Table I gives the used parameters as well as the model comparison numbers $\exp(\mathcal{L})$ normalised to sum to unity. The results show that VMF explains the data better than AE-nominal and AE-fitted models for both Model I and Model II. AE-adaptive attempts to fix the problem of underestimating the azimuth's variance close to the poles, and indeed its model comparison number is close to the VMF model's especially for the normal model with flipping. The fitted maximum likelihood parameters of the AE model show large σ_{AZI} compared to the nominal value because of the influence of the pole areas.

C. A single measurement update example

In this subsection we illustrate the difference of the azimuth–elevation and unit vector based filter updates. We use the prior distribution for the position $\theta \sim \text{N}\left(\begin{bmatrix} 0.3 \\ -0.3 \\ -2 \end{bmatrix}, 0.75^2 I_3\right)$ and a direction measurement $y^{\text{AZI}} = -\pi$, $y^{\text{ELE}} = -\frac{9\pi}{20}$, $\sigma_{\text{AZI}} = \sigma_{\text{ELE}} = 5°\frac{\pi}{180°}$, which gives $\kappa = (\frac{180°}{5°\pi})^2$. The anchor is in the origin. The used UKF parameter is $\lambda = 0.5$, which provides equally weighted sigma points. We have intentionally placed the prior mean and the direction measurement close to and on different sides of the pole.

Fig. 2 shows the example scenario and the filter updates as line segments whose one end is in the prior mean and the other end is in the filtering posterior mean. The figure shows that the VMF filter estimates are in directions close to the measurement direction, which is desirable because the prior distribution is quite diffuse and measurement is the only additional piece of information. The AE filters, on the contrary, update the estimate to an incorrect direction because the measurement model is highly nonlinear close to the pole.
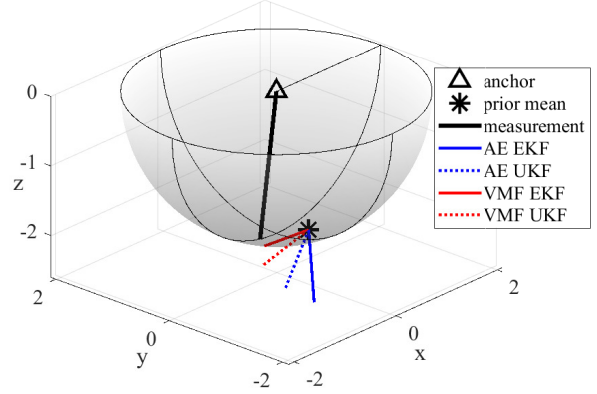

Fig. 2. A single measurement update

In EKF the measurement function is linearised in the prior mean where the azimuth value has steepest descent direction in the clockwise tangential direction of the xy-plane's circle.

D. Positioning tests with simulated data

We designed a $5\,\text{m} \times 5\,\text{m}$ square-shaped test track in the horizontal xy-plane, and four anchors in the same plane. The test scenario was designed such that in two sides of the square the elevations of two anchors are zero. This is done to test how the algorithms perform close to the poles. We generated 10^4 Monte Carlo replications of the test track and the AOA measurements. The travelled distances between the measurement time instants were generated with the model

$$\ell_k \sim \text{N}\Big(q_{xy}\sqrt{2\delta}\,\Gamma(1.5),\, 2q_{xy}^2\delta(1-\Gamma^2(1.5))\Big), \tag{12}$$

where Γ is the Gamma function, the process noise parameter is $q_{xy} = 0.5\,\text{m/s}^{\frac{1}{2}}$, and the time difference is $\delta = 0.25\,\text{s}$. The filter state includes only the user position, i.e. $x_k = \theta_k$, and the state-transition model is the random-walk model

$$\theta_k = \theta_{k-1} + w_{k-1}, \quad w_{k-1} \sim \text{N}\Big(0_3, \delta\begin{bmatrix} q_{xy}^2 I_2 & 0_2 \\ 0_2^\mathsf{T} & q_z^2 \end{bmatrix}\Big), \tag{13}$$

where q_z is the process noise parameter for the z-direction for which we used $q_z = 0.1\,\text{m/s}^{\frac{1}{2}}$. In this model, the random variable $\frac{1}{q_{xy}\sqrt{\delta}}\|[w_k]_{1:2}\|$ follows the chi-distribution with two degrees of freedom χ_2 whose mean is $\sqrt{2}\Gamma(1.5)$ and variance $2(1-\Gamma^2(1.5))$, which gives the basis for the simulation model (12). We used 10^4 particles in PF and the UKF parameter value $\lambda = 0.5$. Fig. 3 shows an example of a simulated test track and the filter estimates. "AE-adaptive" filters use a non-additive measurement noise model where the measurement noise distribution's covariance matrix depends on the elevation through the formula explained in Section IV-B.

Fig. 4 shows the distributions of the percentual root-mean-square error (RMSE) difference from the PF-VMF algorithm's RMSEs. On the left, the measurement errors have been generated from Model I, and on the right from Model II. The box levels are 5%, 25%, 50%, 75%, and 95% quantiles, and the asterisks show the minimum and maximum. The results show
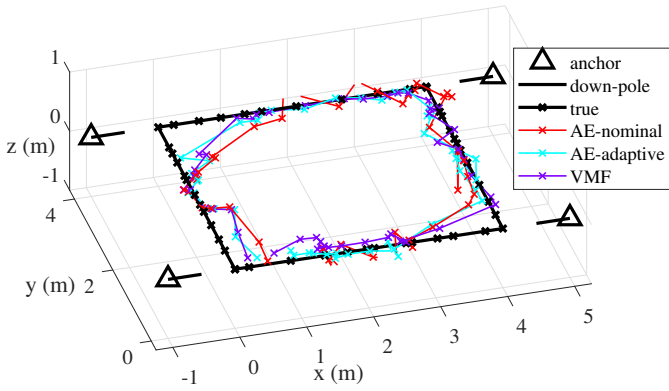
Fig. 3. Test track and axted track with PF estimates. The tracks starts in the origin and goes counter-clockwise.

Fig. 4. Percentual RMSE differences from PF-VMF. The measurement errors are generated from the normal distribution with flipping and $\sigma_{\text{AZI}} = \sigma_{\text{ELE}} = 10°$ (upper), and from the VMF distribution with $\kappa = \left(\frac{180°}{10° \pi}\right)^2$ (lower). The box levels are 5 %, 25 %, 50 %, 75 %, and 95 % quantiles, and the asterisks show the minimum and maximum.

that the VMF based algorithms greatly and systematically outperform the AE algorithms in accuracy. The differences are emphasised with EKF and UKF, which is probably due to the high nonlinearity of the measurement function close to the pole directions as explained in Section IV-C. AE-adaptive filters are closer in accuracy to VMF than AE-nominal and AE-fitted, but in EKF and UKF the adaptivity does not necessarily improve the accuracy. This is probably due to the fact that these filters choose the measurement noise variance locally, in a single point in EKF and in the sigma points in UKF. Furthermore, the VMF based EKF and UKF are close to the VMF based PF in accuracy.

V. CONCLUSION

In this article we propose modelling an angle-of-arrival (AOA) positioning measurement as a von Mises–Fisher (VMF)-distributed unit vector instead of the conventional normally distributed azimuth and elevation measurements. Describing the 2-dimensional AOA measurement with three numbers removes discontinuities and reduces nonlinearity at the poles of the azimuth–elevation coordinate system. Furthermore, in the VMF based model the distribution of the physical measurement errors is invariant of rotations of the spherical coordinate system in which the azimuth and elevation measurements are expressed, which is sound if there is no reason to assume narrower and asymmetric error distributions in solid angle space close to the pole directions. The presented simulations show that when the user moves close to the pole directions, the proposed VMF based particle filter (PF), extended Kalman fiter (EKF), and unscented Kalman filter (UKF) algorithms show substantial improvement in the positioning accuracy.

REFERENCES

[1] M. Koivisto, M. Costa, J. Werner, K. Heiska, J. Talvitie, K. Leppänen, V. Koivunen, and M. Valkama, "Joint device positioning and clock synchronization in 5G ultra-dense networks," *IEEE Transactions on Wireless Communications*, no. 99, 2017.

[2] Quuppa Oy, Quuppa Intelligent Locating System^TM. [Online]. Available: http://quuppa.com/technology/
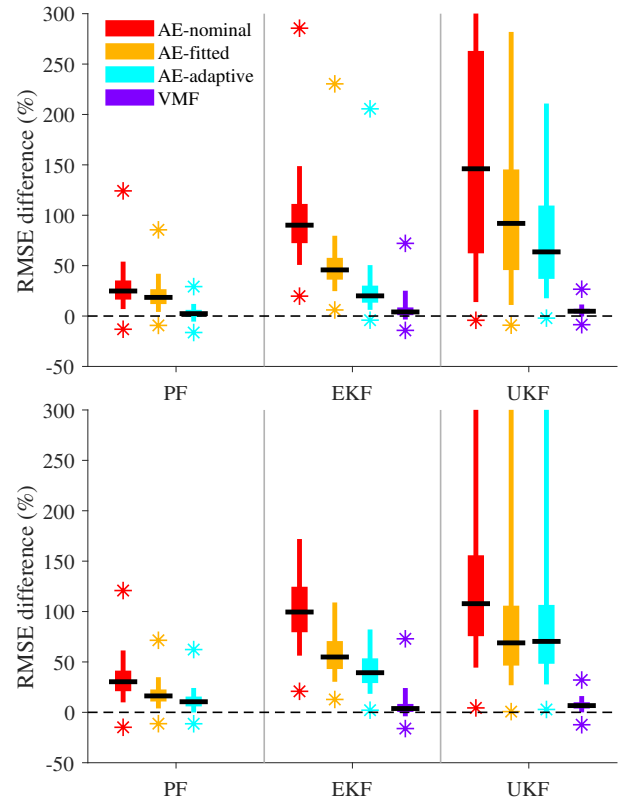
[3] A. Toloei and S. Niazi, "State estimation for target tracking problems with nonlinear Kalman filter algorithms," *International Journal of Computer Applications*, vol. 98, no. 17, pp. 30–36, 2014.

[4] A. Sofyali and C. Hajiyev, "Single station antenna–based spacecraft orbit determination via robust EKF against the effect of measurement matrix singularity," *Journal of Aerospace Engineering*, vol. 28, no. 1, 2015.

[5] B. Huang, Z. Yao, X. Cui, and M. Lu, "Angle-of-arrival assisted GNSS collaborative positioning," *Sensors*, vol. 16, no. 6, June 2016.

[6] M. Ahmed and K. Subbarao, "Target tracking in 3-D using estimation based nonlinear control laws for UAVs," *Aerospace*, vol. 3, no. 1, 2016.

[7] M. Koivisto, A. Hakkarainen, M. Costa, J. Talvitie, K. Heiska, K. Leppänen, and M. Valkama, "Continuous high-accuracy radio positioning of cars in ultra-dense 5G networks," in *IEEE International Wireless Communications and Mobile Computing Conference (IWCMC)*, 2017.

[8] R. Fisher, "Dispersion on a sphere," *Proceedings of the Royal Society of London. Series A, Mathematical and Physical Sciences*, vol. 217, no. 1130, pp. 295–305, 1953.

[9] N. Fisher, T. Lewis, and B. Embleton, *Statistical analysis of spherical data*. Cambridge University Press, 1987.

[10] J. B. Kuipers, *Quaternions and Rotation Sequences*. Princeton, NJ: Princeton University Press, 1999.

[11] I. Gilitschenski, G. Kurz, S. J. Julier, and U. D. Hanebeck, "Unscented orientation estimation based on the Bingham distribution," *IEEE Transactions on Automatic Control*, vol. 61, no. 1, pp. 172–177, January 2016.

[12] N. J. Gordon, D. J. Salmond, and A. F. Smith, "Novel approach to nonlinear/non-Gaussian Bayesian state estimation," *IEE Proceedings F*, vol. 140, no. 2, pp. 107–113, April 1993.

[13] A. H. Jazwinski, *Stochastic Processes and Filtering Theory*, ser. Mathematics in Science and Engineering. Academic Press, 1970, vol. 64.

[14] S. J. Julier, J. K. Uhlmann, and H. F. Durrant-Whyte, "A new approach

for filtering nonlinear systems," in *American Control Conference*, vol. 3, 1995, pp. 1628–1632.

[15] A. Chiuso and G. Picci, "Visual tracking of points as estimation on the unit sphere," in *The confluence of vision and control. Lecture Notes in Control and Information Sciences*, D. Kriegman, G. Hager, and A. Morse, Eds.   London, UK: Springer, 1998, vol. 237.

[16] J. Traa and P. Smaragdis, "Multiple speaker tracking with the factorial von Mises–Fisher filter," in *20th IEEE International Workshop on Machine Learning for Signal Processing (MLSP)*, 2014.

[17] I. Marković, M. Bukal, J. Ćesić, and I. Petrović, "Direction-only tracking of moving objects on the unit sphere via probabilistic data association," in *17th International Conference on Information Fusion (FUSION)*, 2014.

[18] G. Kurz, I. Gilitschenski, and U. D. Hanebeck, "Unscented von Mises–Fisher filtering," *IEEE Signal Processing Letters*, vol. 23, no. 4, pp. 463–467, April 2016.

[19] K. V. Mardia and P. E. Jupp, *Directional Statistics*.   John Wiley & Sons, 2000.

[20] B. Ristic, S. Arulampalam, and N. Gordon, *Beyond the Kalman Filter, Particle Filters for Tracking Applications*.   Boston, London: Artech House, 2004.